

# Catalysis Science & Technology

Accepted Manuscript



This article can be cited before page numbers have been issued, to do this please use: H. Wang, Y. Wang, A. Jia, C. Wang, L. Wu, Y. Yang and Y. Wang, *Catal. Sci. Technol.*, 2017, DOI: 10.1039/C7CY01725A.



This is an Accepted Manuscript, which has been through the Royal Society of Chemistry peer review process and has been accepted for publication.

Accepted Manuscripts are published online shortly after acceptance, before technical editing, formatting and proof reading. Using this free service, authors can make their results available to the community, in citable form, before we publish the edited article. We will replace this Accepted Manuscript with the edited and formatted Advance Article as soon as it is available.

You can find more information about Accepted Manuscripts in the [author guidelines](#).

Please note that technical editing may introduce minor changes to the text and/or graphics, which may alter content. The journal's standard [Terms & Conditions](#) and the ethical guidelines, outlined in our [author and reviewer resource centre](#), still apply. In no event shall the Royal Society of Chemistry be held responsible for any errors or omissions in this Accepted Manuscript or any consequences arising from the use of any information it contains.



## A novel bifunctional Pd-ZIF-8/rGO catalyst with spatially separated active sites for the tandem Knoevenagel condensation-reduction reaction

Received 00th January 20xx,  
Accepted 00th January 20xx

DOI: 10.1039/x0xx00000x

[www.rsc.org/](http://www.rsc.org/)

Hefang Wang,<sup>a</sup> Yansu Wang,<sup>a</sup> Aizhong Jia,<sup>a</sup> Cunyue Wang,<sup>a</sup> Luming Wu,<sup>a</sup> Yongfang Yang\*<sup>a</sup> and Yanji Wang\*<sup>a</sup>

A novel bifunctional catalyst with spatially separated active sites was prepared by the immobilization of Pd nanoparticles (NPs) via covalent interaction and coordination of zeolitic imidazolate framework (ZIF-8) on the surface of graphene oxide (GO), respectively, which was used as an efficient catalyst for the Knoevenagel condensation-reduction tandem reaction. The results of Fourier transform infrared spectroscopy (FT-IR), X-ray diffraction (XRD), Raman spectra, UV-Vis spectra, X-ray photoelectron spectroscopy (XPS) and thermogravimetric analysis (TGA) demonstrated that Pd and ZIF-8 were successfully immobilized on the surface of GO, and the GO was reduced to reduced graphene oxide (rGO) using NaBH<sub>4</sub> as reductant in the preparation of Pd-ZIF-8/rGO. The textural and morphology of Pd-ZIF-8/rGO were characterized by N<sub>2</sub> adsorption-desorption, scanning electronic micrograph (SEM) and transmission electron microscope (TEM). Pd-ZIF-8/rGO shows excellent catalytic performance in the tandem reaction with 100% benzaldehyde conversion and 98.3% selectivity to benzylmalononitrile. The excellent catalytic performance of Pd-ZIF-8/rGO in the tandem reaction is due to the high catalytic activities of spatially separated Pd NPs and ZIF-8 active sites and concentrated reactants on the surface of Pd-ZIF-8/rGO due to the  $\pi$ - $\pi$  interaction between rGO and the reactants. The anchor and stabilization effects of oxygenated groups of GO inhibit the aggregation and leak of active sites, leading to good catalytic recyclability with almost unchanged catalytic activity for more than eight times in the tandem reaction.

School of Chemical Engineering and Technology, Hebei University of Technology,  
Tianjin 300130, China

E-mail address: [wuyuyang123456@163.com](mailto:wuyuyang123456@163.com) (Y. Yang), [yjwang@hebut.edu.cn](mailto:yjwang@hebut.edu.cn) (Y. Wang)

Electronic Supplementary Information (ESI) available: See  
DOI: 10.1039/x0xx00000x

### 1. Introduction

Tandem reactions, which enable multistep reactions in one pot, increase the economic competitiveness in the production of target compounds and the greenness of the process by reducing capital investment, being effective in the minimization of wastes and energy consumption, and

optimizing the use of solvent.<sup>1,2</sup> Benzylmalononitrile is an important pharmaceutical intermediate, which can be used in the synthesis of antimalarials.<sup>3</sup> One-pot synthesis of benzylmalononitrile by tandem Knoevenagel condensation-reduction reaction, as an attractive synthetic method for improving overall process efficiency, has raised extensive interest of researchers. Hantzsch 1,4-dihydropyridine<sup>4</sup> or NaBH<sub>4</sub><sup>5</sup> were used as reductant with 68% and 87% yield in the above process, respectively. However, the use of NaBH<sub>4</sub> had the disadvantages of high reaction cost and the negative impact of borate on the aqueous environment.

Benzylidenemalononitrile was synthesized efficiently from benzaldehyde and malononitrile by Knoevenagel condensation using base catalysts, such as layered double hydroxides (LDHs),<sup>6</sup> amine modified graphene oxide,<sup>7</sup> amine functionalized K10 montmorillonite,<sup>8</sup> graphitic carbon nitride (g-C<sub>3</sub>N<sub>4</sub>),<sup>9,10</sup> zeolites<sup>11</sup> and Metal Organic Frameworks (MOFs) (e.g. IRMOF-3,<sup>12</sup> MIL-101<sup>13</sup> and ZIF-8<sup>14-18</sup>). Among them, ZIF-8 has drawn more attention owing to its outstanding characteristics, such as Zn<sup>2+</sup> as its acidic site and the nitrogen atom of the 2-methylimidazole ligand as its basic site, large surface area, well-defined pore structure, high thermal and chemical stability.<sup>14-18</sup> Previous studies showed that the catalytic activity of ZIF-8 increased significantly with the decrease of the particle size due to almost all active sites located at the external surface of ZIF-8. However, the nanoparticles (NPs) of ZIF-8 were difficult to be recovered and reused after reaction.<sup>19,20</sup>

Pd is usually used as the catalytic center for the reduction of C=C bond in  $\alpha$ ,  $\beta$ -unsaturated compounds. Pd NPs supported on ZIF-8 showed good catalytic activity in the reduction.<sup>21-25</sup> However, the diameter of Pd NPs (2-50 nm) are larger than the cavity of ZIF-8, which has the sodalite (SOD) zeolite structure with large cavities (11.6 Å) and small apertures (3.4 Å). Therefore, most of Pd NPs are dispersed on the exterior surface of ZIF-8, which tend to the migration and aggregation of NPs due to their high surface energy, leading to loss of the catalytic activity during reactions.

The controlled synthesis of bifunctional catalysts, which are active to promote all the individual reactions involved in the tandem reaction, is an effective

strategy.<sup>2,26</sup> However, bifunctional catalysts usually exhibited inferior catalytic activity and durability due to the interaction between separated active sites. Therefore, it is highly desirable to develop a suitable support, which can be used for the high dispersion of the active species and inhibit the interaction between separated active sites effectively. GO is an attractive material because of its unique properties, such as the strong  $\pi$ - $\pi$  interaction between GO and reactants, various oxygenated groups such as hydroxyl, epoxy or carboxyl groups and high surface area (2000 m<sup>2</sup>/g).<sup>27</sup> The surface oxygenated groups and defects on GO can act as nucleation sites to anchor the Pd NPs<sup>28-30</sup> and can also coordinate with Zn<sup>2+</sup> ions<sup>31,32</sup>, which are the precursors of ZIF-8. The anchor and stabilization effects of the oxygenated groups and defects on GO could prevent the aggregation and leak of Pd NPs and ZIF-8. A 2D structure of GO also facilitates the diffusion/transportation of reactant and product and the utilization of active site in the Knoevenagel condensation-reduction tandem reaction. Therefore, GO can be used as an ideal support for ZIF-8 and Pd NPs.<sup>33-35</sup>

Herein, Pd-ZIF-8/rGO was prepared by the immobilization of Pd NPs via covalent interaction and coordination of ZIF-8 on the surface of GO respectively and the Pd-ZIF-8/rGO was used as catalyst in the Knoevenagel condensation-reduction tandem reaction (Scheme 1). As a heterogeneous catalyst, Pd-ZIF-8/rGO can be easily recovered and reused without leak of Pd and ZIF-8.

## 2. Experimental

### 2.1 Materials

All the reagents were analytical purity and were used as received without further purification. Natural flake graphite with an average particle size of 40  $\mu$ m (99%) was purchased from Qingdao Guangyao Graphite Co. Ltd China. Sulfuric acid (98%) and hydrochloric acid (37%) were obtained from Tianjin Institute of Chemical Agents China. 2-Methylimidazole (99.0%) and zinc nitrate hexahydrate (Zn(NO<sub>3</sub>)<sub>2</sub>·6H<sub>2</sub>O) were purchased from Alfa Aesar. Fuming nitric acid (>90%), palladium chloride, sodium hydroxide, sodium borohydride, polyvinyl-

pyrrolidone (PVP) and hydrogen peroxide (30 wt%) were purchased from Tianjin FengChuan Chem. Co. Ltd China. Potassium permanganate was purchased from Hebei Wuluo Pharmaceutical Co. Ltd China. Methanol, ethyl cyanocetate and diethyl malonate were obtained from Tianjin Guangfu Fine Chemical Research Institute China. Malononitrile, 4-methylbenzaldehyde, 4-methoxybenzaldehyde, 4-fluorobenzaldehyde, 4-bromobenzaldehyde and 4-hydroxybenzaldehyde were purchased from Energy Chem. Co. Ltd China.

## 2.2 Characterization

Fourier transform infrared (FT-IR) spectra were collected using the KBr pellet technique on the transmission module of a Bruker Vector 22 FT-IR spectrometer at 2  $\text{cm}^{-1}$  resolution and 64 scans. X-Ray diffraction (XRD) was performed on a D8 Discover (Bruker AXS Ltd.) under ambient conditions using a Cu  $K\alpha$  X-ray. The measurements of Raman spectra were performed on a inVia Reflex (Renishaw) Raman apparatus, using a 532 nm laser beam with a laser power of 1 mW and a detector data acquisition time of 10 s. The UV-vis spectra were acquired on a UV-Vis-NIR L5 spectrophotometer in the range of 200-700 nm. Thermogravimetric analysis (TGA) was conducted on the TGA/DTA system (TA2000, DuPont) from 25°C to 700 °C in a 100 mL/min air flow and a ramp rate of 10 °C/min.  $\text{N}_2$  adsorption-desorption was performed at 77 K on a Micromeritics ASAP2020M+C. All samples were degassed at 160 °C for 18 h. The specific surface area was calculated by the Brunauer-Emmett-Teller (BET) method. The total pore volume and average pore size were calculated from nitrogen desorption isotherm by the Horvath-Kawazoe method. X-ray photoelectron spectroscopy (XPS) was carried out on a Thermo ESCALAB 250XI spectrometer with monochromatic Al  $K\alpha$  radiation. Scanning electron microscopy (SEM) and energy dispersive spectroscopy (EDS) were obtained on a FEI Nova Nano SEM450. Transmission Electron Microscope (TEM) images were acquired on the JEM-2100 microscopy. The palladium content was determined by inductively coupled plasma emission spectroscopy (ICP-AES) on Opfima 7300V (Perkin Elmer). For ICP analyses, the samples were

digested in 10% (v/v) nitric acid solution at 60 °C for 1.0 h. The dispersion of Pd was calculated by the basis of CO adsorption on AutoChem II 2920 chemical analyzer (Norcross, GA, USA) equipped with thermal conductivity detector (TCD) Sample (0.50 g) was first pretreated in 10%  $\text{H}_2/\text{N}_2$  (50  $\text{cm}^3/\text{min}$ ) at 250 °C for 2.0 h and purged with helium (50  $\text{cm}^3/\text{min}$ ) for 1.0 h at the same temperature. And then, the catalyst was cooled to 60 °C and CO pulses were injected from a calibrated on-line sampling valve. CO adsorption was assumed to be completed after three successive peaks showed the same peak areas. A CO/Pd stoichiometry of 1 was used for calculations.  $\text{H}_2$ -TPR experiments were also performed on AutoChem II 2920 chemical analyzer. A catalyst sample (0.10 g) was previously heated for 1.0 h at 250 °C under an Ar stream, and then cooled to 60 °C. Hydrogen consumption was calculated in the flow of 10%  $\text{H}_2/\text{Ar}$  gas mixture at 50 mL/min and the temperature was raised up to 300 °C with a heating rate of 10 °C/min.

## 2.3 Catalysts preparation

**2.3.1 Preparation of ZIF-8.** ZIF-8 was prepared according to the reported procedure.<sup>32</sup> Typically, 744 mg of  $\text{Zn}(\text{NO}_3)_2 \cdot 6\text{H}_2\text{O}$  and 411 mg of 2-methylimidazole were dissolved in 50 mL of methanol, respectively. Then the zinc nitrate solution was mixed with the 2-methylimidazole solution and stirred for 1.0 h at 25 °C. The molar ratios of metal: ligand: MeOH were 1:2:1250. The resultant mixture was centrifuged and washed three times with deionized water, then dried for 12.0 h in a vacuum oven (60 °C, -0.1 MPa). Finally, the ZIF-8 was obtained.

**2.3.2 Preparation of ZIF-8/GO.** GO was prepared by oxidation of graphite powder according to the reported Hummers method.<sup>36</sup> Firstly, a certain amount of GO was dispersed in deionized water and sonicated for 2.0 h at 25 °C. 744 mg of  $\text{Zn}(\text{NO}_3)_2 \cdot 6\text{H}_2\text{O}$  and 411 mg of 2-methylimidazole were dissolved in 50 mL of methanol, respectively. Secondly, the methanol solution of zinc nitrate was mixed with solution of GO and stirred at 25 °C for 1.0 h. Afterwards, the methanol solution of 2-methylimidazole was added into the above solution under

stirring at 25 °C for 1.0 h. The resultant mixture was centrifuged and washed three times with deionized water, then dried for 12.0 h in a vacuum oven (60 °C, -0.1 MPa). Finally, the ZIF-8/GO was obtained.

**2.3.3 Preparation of Pd-ZIF-8/rGO.** Pd-ZIF-8/rGO was prepared by the immobilization of ZIF-8 via coordination and covalent interaction of Pd NPs on the surface of GO, respectively. As illustrated in Scheme 2, firstly, Zn<sup>2+</sup> ions were coordinated with the oxygen-containing functional groups of GO. Then, 2-methylimidazole coordinate with Zn<sup>2+</sup> to form ZIF-8/GO. Finally, Pd NPs were anchored and stabilized by oxygenated groups of GO with the protection of PVP during the reduction of NaBH<sub>4</sub>. Typically, the PdCl<sub>2</sub> was dissolved in HCl, and NaOH was then added under stirring until the pH=7 obtaining the Na<sub>2</sub>PdCl<sub>4</sub> solution (0.01 M). Then, 11.29 mg of polyvinyl-pyrrolidone (PVP) was added to the PdCl<sub>2</sub> solution (2.56 mL, 0.01 M) at 25 °C. After stirring for 1.0 h, 100 mg of the dried ZIF-8/GO was added into the above solution and the mixture was stirred for 2.0 h. Then, 1.28 mL of NaBH<sub>4</sub> solution (0.1 M) was added dropwise into the reaction mixture with vigorous stirring at 0 °C. After further stirring for 5.0 h, the resultant mixture was isolated by filtration and washed three times with deionized water. Then, the obtained product was dried for 12.0 h in a vacuum oven (60 °C, -0.1 MPa). The product is named as Pd-ZIF-8/rGO due to the fact that GO was reduced during the preparation process.

**2.3.4 Preparation of Pd/(ZIF-8+rGO).** For comparison, Pd/(ZIF-8+rGO) was prepared by immobilization of Pd particles onto the physical mixture of ZIF-8 and GO. Typically, 75 mg of the dried ZIF-8 was added into the GO dispersion (5.0 mg/mL) and the mixture was stirred for 2.0 h (ZIF-8+GO). Then, the above mixture was added into the Na<sub>2</sub>PdCl<sub>4</sub> solution (2.56 mL, 0.01 M) with 11.29 mg of polyvinyl-pyrrolidone (PVP) at 25 °C and the mixture was stirred for 2.0 h. Afterwards, 1.28 mL of NaBH<sub>4</sub> solution (0.1 M) was added dropwise into the above mixture with vigorous stirring at 0 °C for 5.0 h. The resultant mixture was isolated by filtration, washed three times with deionized water and dried for 12.0 h in a vacuum oven (60 °C, -0.1 MPa).

All the samples have the same Pd loading. For comparison, the rGO and ZIF-8/rGO were also prepared with the same procedure. The detailed synthesis procedures of Pd/ZIF-8 and Pd/rGO are shown in SI.

## 2.4 One-pot tandem reaction

The one-pot tandem Knoevenagel condensation-reduction reaction was carried out in a 25 mL three-necked round flask equipped with a magnetic stirrer, a reflux condenser and a hydrogen balloon. Typically, 40 mg of catalyst, 5.0 mL toluene, 1.9 mmol of benzaldehyde and 3.8 mmol malononitrile were added to the reactor. Then the mixture was stirred and heated at 60 °C for 4.0 h under air atmosphere. Subsequently, the reactor was purged with H<sub>2</sub> to remove the air for five times and then the reactor was sealed. The reaction mixture was further stirred for 12.0 h at the same temperature under H<sub>2</sub> atmosphere. After the reaction, the remaining H<sub>2</sub> was removed by a careful venting process, then the mixture was separated by centrifugation. The organic phase was confirmed by a Thermo Trace DSQ gas chromatograph-mass spectrometer and product was analyzed by a SP-3420A gas chromatograph equipped with a KB-Wax column (30 m, 0.32 mm id, 0.25 μm film thickness) with decane as internal standard. The recovered catalysts were washed with ethanol and deionized water and then dried for 12.0 h in a vacuum oven (60 °C, -0.1 MPa) before reuse.

## 3. Results and discussion

### 3.1 Catalyst characterization

**3.1.1 Compositional and structural information of Pd-ZIF-8/rGO.** The FT-IR spectra of rGO, ZIF-8, ZIF-8/GO and Pd-ZIF-8/rGO samples are shown in Fig. 1a. The FT-IR spectrum of rGO shows two peaks at 1050 cm<sup>-1</sup> and 1390 cm<sup>-1</sup>, corresponding to the C-O stretching and O-H bend vibration, respectively,<sup>28,30</sup> which indicates significant reduction of all oxygen containing groups by NaBH<sub>4</sub>. Similar results were also obtained by Wojtoniszak.<sup>37</sup> For the spectrum of ZIF-8, the adsorption peak at 1578 cm<sup>-1</sup> is associated with the C=N stretching vibrations of the imidazole, whereas the intense and convoluted peak at 1421 cm<sup>-1</sup> is ascribed to the entire ring

stretching.<sup>38</sup> The peaks at 1306, 1145 and 998  $\text{cm}^{-1}$  are attributed to the in-plane bending of the ring, while the peak at 750  $\text{cm}^{-1}$  is attributed to out-of-plane bending.<sup>39</sup> In addition, the peak at 421  $\text{cm}^{-1}$  may be related to the Zn-N stretch mode.<sup>40,41</sup> The above characteristic peaks of ZIF-8 are obviously observed in the FT-IR spectra of ZIF-8/GO and Pd-ZIF-8/rGO, indicating that the immobilization of GO and Pd does not disturb the coordination of 2-methylimidazole linker to the zinc(II) centers and thus the formation of ZIF-8. However, the vibration peaks related to functional groups of rGO are not observed in Pd-ZIF-8/rGO, which is probably due to the weak absorption peaks and high dispersion of rGO.<sup>37</sup>

The powder XRD patterns of as-synthesized GO, rGO, ZIF-8, ZIF-8/GO and Pd-ZIF-8/rGO samples are shown in Fig. 1b. For GO, the peak located at 12.5° ( $d = 0.71$  nm) is attributed to (002) crystal plane of the layered structure of GO. The large interlayer distance is attributed to the formation of hydroxyl, epoxy and carboxyl groups, which increase the distance between the layers.<sup>42-44</sup> However, the disappearance of the peak at 12.5° and the presence of a new broad diffraction peak at 23.7° ( $d = 0.37$  nm) in the spectra of rGO indicate the reduction of GO to rGO.<sup>45,46</sup> For the spectrum of ZIF-8/GO, no characteristic diffraction peaks of GO are observed, which is attributed to that the high intensity of ZIF-8 peak at 12.4° overlapped the characteristic peak of GO at 12.5°.<sup>47</sup> For the spectrum of Pd-ZIF-8/rGO, no characteristic diffraction peaks of rGO are observed, which is probably due to the high dispersion of rGO in the composite.<sup>48</sup> The diffraction patterns of ZIF-8 are in agreement with the previous reports,<sup>46,49</sup> confirming the formation of pure crystalline ZIF-8 phase. The typical peaks of ZIF-8 in the XRD patterns of ZIF-8/GO and Pd-ZIF-8/rGO indicate that ZIF-8 is successfully immobilized onto the surface of GO and its structure is well preserved. According to the Scherrer equation, the average ZIF-8 particle sizes of pure ZIF-8, ZIF-8/GO and Pd-ZIF-8/rGO are 94, 53 and 56 nm, respectively, which could be probably ascribed to that -OH and -COOH groups inhibit the growth of large crystals of ZIF-8 through coordination modulation.<sup>31,50</sup> Small particle size of ZIF-8 anchored on GO could have good catalytic activity in Knoevenagel condensation. In addition, no

characteristic diffraction peaks of Pd are observed in the XRD patterns of Pd-ZIF-8/rGO, which is mainly due to the high dispersion of the ultrasmall Pd NPs (~2.8 nm) in the composite, which was also proved by the results of TEM and CO adsorption. Similar conclusion was also obtained in case of the immobilization of Pt NPs on the ZIF-8/GO support via a facile liquid impregnation method.<sup>51</sup> Additionally, the intensity of the diffraction peaks of Pd-ZIF-8/rGO is weaker than that of ZIF-8 and ZIF-8/GO, which could be due to the changes in the charge distribution and electrostatic fields as the result of the existence of Pd NPs on the surface and interaction of their electrophilic surface with framework atoms.<sup>52</sup>

Raman spectroscopy is a widely used and reliable technique to characterize the structural changes that occur before and after the reduction of GO. Raman spectra of the GO, ZIF-8 and Pd-ZIF-8/rGO are presented in Fig. 1c. The peaks at 685, 1142, 1184, 1460 and 1509  $\text{cm}^{-1}$  in the spectra of ZIF-8 are assigned to the vibrational mode of the 2-methylimidazolate ligand.<sup>53</sup> The Raman spectrum of GO exhibits two feature peaks at 1337 and 1596  $\text{cm}^{-1}$ , which are attributed to the D and G bands, respectively.<sup>40</sup> The G band represents the vibration of graphitic ( $\text{sp}^2$  carbon) lattice, while the D band indicates the defects and disordered regions of the lattice caused by oxidation reaction.<sup>54,55</sup> The intensity ratio of D band to G band ( $I_D/I_G$ ) indicates the degree of structural defects and a quantitative measurement of edge plane exposure.<sup>56</sup> For Pd-ZIF-8/rGO, no obvious peaks of the ZIF-8 bands are observed in Raman spectra except for the appearance of bands associated with GO owing to the strong intensity of GO. The Raman spectra of Pd-ZIF-8/rGO show higher  $I_D/I_G$  (1.22) than that of GO (0.99), indicating that the GO is reduced to rGO during the information of Pd-ZIF-8/rGO using  $\text{NaBH}_4$  as reductant.<sup>54</sup> The result is consistent with the results of FT-IR and XRD.

The UV-Vis absorption spectra are used to study the interaction between ZIF-8 and GO. Fig. 1d shows the UV-Vis absorption spectra of GO, ZIF-8, ZIF-8/GO and Pd-ZIF-8/rGO dispersed in deionized water. The absorption peak of GO at 233 nm and a shoulder peak at about 300 nm could be assigned to the  $\pi \rightarrow \pi^*$  transitions of aromatic C-C bonds and the  $n \rightarrow \pi^*$  transitions of C=O bonds, respectively. The results are in agreement with the

results of Zhang<sup>57</sup> and Jahan<sup>58</sup>. The UV-Vis absorption spectrum of pristine ZIF-8 has an absorption band at 204 nm, while the UV-Vis absorption spectrum of ZIF-8/GO and Pd-ZIF-8/rGO composites shows a slight shift in absorption band at 205 nm and 206 nm compared with that of pristine ZIF-8.<sup>59</sup> This red shift in the absorption band could be due to the charge or energy transfer interaction between the polyaromatic scaffold in GO and ZIF-8,<sup>58,59</sup> suggesting the existence of the coordination interaction between the GO and ZIF-8 in the in situ synthesized ZIF-8/GO and Pd-ZIF-8/rGO composites, which is consistent with the results of XRD.

XPS was performed to further investigate the interaction between active sites (ZIF-8 and Pd) and rGO in Pd-ZIF-8/rGO. The XPS wide scan spectrum shows that Pd-ZIF-8/rGO is composed of C, N, O, Zn and Pd (Fig. 2a). The existences of Zn and Pd indicate that ZIF-8 and Pd are successfully immobilized on the surface of rGO. The C 1s XPS spectrum of GO display four characteristic peaks at 284.8 eV, 286.6 eV, 287.0 eV and 288.2 eV (Fig. 2b), attributed to C-C/C=C, C-O, C=O and O-C=O, respectively, which are in agreement with the results reported previously.<sup>60-62</sup> For the XPS spectra of ZIF-8, the C 1s spectra can be deconvoluted into two peaks at 284.6 eV and 285.4 eV (Fig. 2c), corresponding to the C-C bond and C-N bond, respectively.<sup>19</sup> The C 1s peaks of ZIF-8 and the C=O bond of GO are observed in the C 1s XPS spectrum of ZIF-8/GO, however, other functional groups (C-C/C=C, C-O and O-C=O) disappear in comparison with those of GO, which is attributed to the chemical interaction between ZIF-8 and GO. The similar results were also obtained by Luanwuth.<sup>40</sup> As shown in Fig. 2e, a strong peak at 284.7 eV (C=C/C-C) is dominant and the peak intensity of C=O decreases significantly compared with those of ZIF-8/GO, indicating that the GO component is reduced to rGO by NaBH<sub>4</sub>. Moreover, a new C 1s peak at 291.4 eV corresponding to Pd-C bond is observed in comparison with that of ZIF-8/GO, indicating the existence of covalent interaction between the Pd NPs and the surface carbon atom of GO in Pd-ZIF-8/rGO.<sup>63</sup> Similar results were reported by Yan and coworkers,<sup>64</sup> which confirmed covalent interaction between the Pd NPs and graphene by IR spectroscopy for the first time. Fig. 2f shows the

characteristic peaks at 340.5 eV and 335.3 eV for Pd 3d, which are attributed to Pd<sup>0</sup> (3d<sub>3/2</sub>) and Pd<sup>0</sup> (3d<sub>5/2</sub>), respectively. Meanwhile, peaks at 343.2 eV and 338.2 eV are attributed to Pd<sup>2+</sup> (3d<sub>3/2</sub>) and Pd<sup>2+</sup> (3d<sub>5/2</sub>), respectively. The area ratio of Pd<sup>0</sup>: Pd<sup>2+</sup> is about 7.3:1, demonstrating that most of Pd<sup>2+</sup> on the surface of the Pd-ZIF-8/rGO was reduced.<sup>30,44</sup>

Graphene oxide is known to interact with supported metal components affecting the catalyst's properties and subsequently its catalytic performance. Therefore, H<sub>2</sub>-TPR of Pd-ZIF-8/rGO catalyst can provide information on the interactions between the Pd and rGO anchored with ZIF-8. Fig. 3 shows the H<sub>2</sub>-TPR profiles of Pd/ZIF-8, Pd/(ZIF-8+rGO) and Pd-ZIF-8/rGO carried out under identical operating conditions, indicating the reduction behavior of incorporated Pd NPs. The H<sub>2</sub>-TPR profile of Pd/ZIF-8 shows a broad peak (centered at 176 °C) corresponds to the reduction of PdO particles.<sup>65</sup> However, the reduction temperature of PdO in Pd/(ZIF-8+rGO) and Pd-ZIF-8/rGO decreases to 168 °C. The observed decrease in the reduction temperature is attributed to the smaller PdO particles of Pd/(ZIF-8+rGO) and Pd-ZIF-8/rGO, which are more easy to be reduced.<sup>66</sup> As observed from the H<sub>2</sub>-TPR profiles in Fig. 3, the quantification of consumed hydrogen of Pd-ZIF-8/rGO (2.96 mmol H<sub>2</sub>/g) is higher than that of Pd/ZIF-8 (1.29 mmol H<sub>2</sub>/g) and Pd/(ZIF-8+rGO) (1.87 mmol H<sub>2</sub>/g). These results suggest that Pd-ZIF-8/rGO shows strong covalent interaction between the Pd NPs and the surface carbon atom of GO in Pd-ZIF-8/rGO.<sup>67</sup> This strong interaction is essential for the dispersion of the Pd NPs and consequently the high catalytic activity and recyclability of the Pd-ZIF-8/rGO catalysts.

The TGA curves of rGO, ZIF-8, ZIF-8/rGO and Pd-ZIF-8/rGO are shown in Fig. 4. The TGA curve of rGO shows two weight loss steps. The first weight loss of about 44.5% between 25 °C and 250 °C corresponds to the removal of oxygen-containing functional groups.<sup>68</sup> The second weight loss of about 55.5% between 250 °C and 500 °C is due to the decomposition of the carbon skeleton.<sup>54,68</sup> For ZIF-8, a small weight loss of about 7.10% up to 250 °C corresponds to the removal of adsorbed water and other absorbed unreacted molecules, and the weight loss of 61.6% from 250 to 650 °C is

attributed to the structural degradation and decomposition of organic ligands. The final white solid residue was identified as ZnO by XRD according to the report of Luanwuthi.<sup>40</sup> The TGA curves also show that ZIF-8/rGO and Pd-ZIF-8/rGO composites have excellent chemical stability between 25 to 200 °C with the small weight loss about 4.05% and 2.12%, respectively. According to the above results, the Pd, ZIF-8 and rGO content in Pd-ZIF-8/rGO are about 11.8%, 78.4% and 7.63%, respectively. Additionally, Pd loading determined by ICP-AES is about 12.5%, which is similar to the result of TGA.

**3.1.2 Morphology and textural property of GO, ZIF-8, ZIF-8/GO and Pd-ZIF-8/rGO.** The N<sub>2</sub> adsorption-desorption isotherms and the corresponding pore size distribution curves (PSD curves) of ZIF-8, ZIF-8/GO and Pd-ZIF-8/rGO are shown in Fig. 5. A typical Type I isotherm with a steep increase at low relative pressures (< 0.01) indicates that all ZIF-8 composites are microporous.<sup>46</sup> The hysteresis loops indicating the existence of mesoporous structures corresponding to the central cavities in ZIF-8 composites and inevitable voids between neighboring ZIF-8 nanocrystals.<sup>32,52,69</sup> The corresponding PSD curves of ZIF-8, ZIF-8/GO and Pd-ZIF-8/rGO also show that the samples exhibit a dominant pore diameter of approximately 0.66 nm (Fig. 5 inset). The specific surface area, the micropore volume and the pore size of ZIF-8 are 1417 m<sup>2</sup>/g, 0.58 cm<sup>3</sup>/g and 0.66 nm, respectively (Table 1), which are very close to the results in the previous reports.<sup>60,70</sup> For ZIF-8/GO, the decreases in BET surface area and pore volume compared with those of ZIF-8 are due to the introduction of GO to ZIF-8 (shown in Table 1). For Pd-ZIF-8/rGO, a slight decrease in BET surface area compared with that of ZIF-8/GO is observed, which might be due to the introduction of Pd NPs to ZIF-8/GO (Table 1).<sup>71</sup> However, the incorporation of Pd NPs does not alter the pore-size distribution of the ZIF-8/GO, consistent with the fact that the Pd NPs are anchored on the surface of rGO (Fig. 5 inset).

The morphology of GO, ZIF-8, ZIF-8/GO and Pd-ZIF-8/rGO was observed by SEM and TEM (Fig. 6). The SEM image of GO exhibits curled and corrugated layered structure. Fig. 6b shows SEM image of ZIF-8, in which the ZIF-8 exhibits a hexagonal shape with an average

particle size of ~90 nm. Fig. 6c and d show SEM images of ZIF-8/GO and Pd-ZIF-8/rGO, in which the ZIF-8 can be observed as irregular hexagons with ~50 nm size covered the GO sheets. Pd NPs in Pd-ZIF-8/rGO can not be observed in the SEM image due to their small size. Fig. 6e shows TEM image of Pd-ZIF-8/rGO, in which the curled and corrugated layered sheets of GO and spherical morphology of ZIF-8 are clearly observed. Furthermore, Pd NPs also can be observed obviously as black dots with an average size of approximately 2.8 nm calculated from a statistical evaluation of 100 particles, suggesting that Pd NPs are effectively immobilized onto the GO sheets (Fig. 6g). No significant aggregation of Pd NPs is observed in Pd-ZIF-8/rGO, which is mainly attributed to the fact that PVP was a protecting agent in the course of preparation. In addition, the diameter of Pd NPs is larger than the diameter of the channel or the cavity inside the ZIF-8 (the large pores with diameters of 1.16 Å). Therefore, these large Pd NPs cannot enter the pores of ZIF-8. Fig. 6f shows that the Pd NPs are crystalline with a spacing of 0.224 nm, corresponding to the Pd (111) inter-planar spacing.<sup>72</sup> In addition, the EDS spectra of the Pd-ZIF-8/rGO composite clearly show that the material consists of C, O, N, Zn and Pd, further indicating that ZIF-8 and Pd are successfully immobilized on the surface of rGO (Fig. 6h).

The above characterization results indicate that ZIF-8 and Pd NPs were successfully immobilized on the surface of rGO by the coordination and covalent interaction, respectively. In addition, ZIF-8 and Pd NPs are well-distributed on the rGO, the unique structure of which can provide high surface area and high catalytic activity.

### 3.2 Catalytic Activity

Pd-ZIF-8/rGO was used as catalyst for one-pot synthesis of benzylmalononitrile (Scheme 1). The tandem reaction involves two separate steps: 1) Knoevenagel condensation between benzaldehyde (**A**<sub>1</sub>) and malononitrile to benzylidenemalononitrile (**B**<sub>1</sub>) and 2) the reduction of benzylidenemalononitrile (**B**<sub>1</sub>) to benzylmalononitrile (**C**<sub>1</sub>) under H<sub>2</sub>.

The first Knoevenagel condensation step could be very important for the Knoevenagel condensation-

reduction tandem reaction. For comparison, GO, ZIF-8, ZIF-8+GO (a physical mixture of GO and ZIF-8) and ZIF-8/GO were used as catalysts in Knoevenagel condensation (Fig. 7). The conversions of benzaldehyde are 11.0%, 35.3%, 31.2% and 80.1% over GO, ZIF-8, ZIF-8+GO and ZIF-8/GO in 2.0 h, respectively (Fig. 7). The low conversion of benzaldehyde over GO primarily due to its weak acidity of GO. The conversion of benzaldehyde reached nearly 100% over ZIF-8/GO within 4.0 h. Whereas, the conversion of benzaldehyde reached nearly 100% over ZIF-8 and ZIF-8+GO after 6.0 h and 8.0 h under the same conditions, respectively. A physical mixture of GO and ZIF-8 can also promote the Knoevenagel condensation reaction, but it was not as efficient as the ZIF-8 and ZIF-8/GO catalyst probably due to the increased diffusion limitations. The results demonstrate that ZIF-8/GO exhibits higher catalytic activity than that of GO, ZIF-8 and ZIF-8+GO in the Knoevenagel condensation reaction. The better condensation activity of the ZIF-8/GO was due to the  $\pi$ - $\pi$  interaction between GO and reactants (benzaldehyde and malononitrile) and a good dispersion of ZIF-8 on GO.

Then Pd NPs were immobilized onto the ZIF-8/GO to form a bifunctional Pd-ZIF-8/rGO catalyst for the tandem synthesis of benzylmalononitrile. Also, for comparison, Pd/ZIF-8, Pd/rGO and Pd/(ZIF-8+rGO) were prepared by the same procedure using NaBH<sub>4</sub> as reductant. The Pd loading determined by ICP-AES are 12.3%, 11.9%, 13.2% and 12.5% for Pd/rGO, Pd/ZIF-8, Pd/(ZIF-8+rGO) and Pd/ZIF-8/rGO, respectively. The dispersion of Pd NPs that calculated on the basis of CO adsorption is summarized in Table 2. The degree of Pd dispersion of Pd-ZIF-8/rGO is higher than that of Pd/ZIF-8 and Pd/(ZIF-8+rGO), which are also in accordance with the total selectivity towards the products C<sub>1</sub>. Moreover, no apparent aggregation is found for the Pd NPs with uniform dispersion in Pd-ZIF-8/rGO (Fig. 8), however, there is obvious aggregation of the Pd NPs in Pd/(ZIF-8+rGO) (Fig. S1). Thus the aggregation could be contributed to the degree of Pd dispersion. The Pd NPs sizes of Pd-ZIF-8/rGO are smaller than those of Pd/ZIF-8 and Pd/(ZIF-8+rGO), which are attributed to the strong covalent interaction between the Pd NPs and the surface carbon atom of GO.<sup>66</sup> Therefore, the higher Pd dispersion

than Pd loading for Pd-ZIF-8/rGO was due to the strong covalent interaction between the Pd NPs and the surface carbon atom of GO, which facilitated good dispersion of Pd NPs and also promote the reduction reaction effectively.

The results of CO adsorption indicate that the surface of GO anchored with ZIF-8 favors the anchor of Pd NPs. The effects of reaction conditions such as reaction time, temperature and catalyst amount on the catalytic activities were investigated (Fig. S2). The optimized reaction conditions are reaction time 4+12 h (4.0 h for Knoevenagel condensation and 12.0 h for reduction), reaction temperature at 60 °C and catalyst amount of 40 mg. Then under the optimized reaction conditions, the one-pot synthesis of A<sub>1</sub> over the above catalysts using toluene as solvent were investigated (Fig. 8). No C<sub>1</sub> was formed in the presence of Pd/rGO due to no active sites for Knoevenagel condensation. As expected, Pd-ZIF-8/rGO showed the best catalytic activity towards the Knoevenagel condensation-reduction reaction with ~99% benzaldehyde conversion, which is much higher than those of both Pd/ZIF-8 (68.5%) and Pd/(ZIF-8+rGO) (78.4%). The high conversion of benzaldehyde over Pd-ZIF-8/rGO in the tandem reaction is attributed to the good catalytic performance of ZIF-8 and Pd NPs in the Knoevenagel condensation and reduction, respectively. Moreover, the good dispersion and small sizes of ZIF-8 and Pd NPs also promote the tandem reaction effectively. In addition, the high selectivity to C<sub>1</sub> (98.3%) over Pd-ZIF-8/rGO towards the Knoevenagel condensation-reduction reaction is due to the acidic sites of the rGO and ZIF-8. The same results were also obtained by Zhang.<sup>73</sup> Therefore, the above results suggest that the Pd-ZIF-8/rGO could be used as the desired bifunctional catalyst with spatially separated active sites for both Knoevenagel condensation and reduction reaction in a one-pot reactor.

In order to determine the general applicability and efficiency of the Pd-ZIF-8/rGO in the tandem reactions with different substrates, various benzaldehyde derivatives (A) and active methylene compounds were investigated (Table 3). Introduction electron donor groups at the para-position of the benzaldehyde did not affect the high activities (Table 3, entries 2, 3 and 4) with

appropriate prolonged reaction time. However, when the electron withdrawing group substituted at the para-position, **A** was efficiently converted to the corresponding products (**B**) in only 3.0 h (Table 3, entries 5 and 6), which indicated that the electron withdrawing group was benefit for the Knoevenagel reaction.<sup>14,74</sup> On the other hand, when the condensation reactant malononitrile was substituted by ethyl cyanoacetate or diethyl malonate, the yield for **C** decreased moderately (Table 3, entries 7 and 8), because malononitrile is the most active methylene compound among the three used condensation substrates.<sup>19,75</sup>

### 3.3 Catalyst recycling

An important issue associated with the performance of a heterogeneous catalyst is its recovery and reusability. The Pd-ZIF-8/rGO catalyst could be easily separated by centrifugation after reaction. To investigate the recyclability of the Pd-ZIF-8/rGO catalyst, the catalyst was recycled eight times. As summarized in Fig. 9A, no obvious decrease of the benzaldehyde conversion and the selectivity to benzylmalononitrile during the eight times reuse. In order to confirm that the active species are not the ZIF-8 and Pd leaking from Pd-ZIF-8/rGO catalyst in the Knoevenagel condensation and reduction reaction, hot filtration experiments were carried out. For Knoevenagel condensation, after 0.5 h reaction time, the catalyst was filtered, and reaction solution was kept on stirring under the same reaction conditions. The conversion of benzaldehyde almost remained constantly during the period of 0.5 h to 4.0 h (Fig. 9B). For reduction reaction, after 5.0 h reaction time, the catalyst was filtered, and reaction solution was kept on stirring under the same reaction conditions. The conversion of benzylidenemalononitrile almost remained unchanged during the period of 5.0 h to 16.0 h (Fig. 9C). Additionally, no leaking of the Zn<sup>2+</sup> and Pd occurred in the filtrates after removing catalysts according to the result of ICP-AES. The FT-IR spectra (Fig. 1a) and XRD pattern (Fig. 1b) of recovered Pd-ZIF-8/rGO (R-Pd-ZIF-8/rGO) catalyst after the eighth run showed no significant differences compared with those of the fresh catalyst, indicating the good reusability of the catalyst in the

tandem reaction. Combined with the results of catalytic performance of the reused catalyst, leaking test, FT-IR and XRD, Pd-ZIF-8/rGO catalyst is recoverable and recyclable. The anchor and stabilization effects of the surface oxygen functional groups and defects on GO could prevent the aggregation and leak of Pd NPs and ZIF-8, facilitating the recyclability and the heterogenization of the active sites.

### 4. Conclusions

A bifunctional Pd-ZIF-8/rGO with spatially separated active sites was prepared by a facile impregnation method via coordination of ZIF-8 and covalent interaction of Pd on the surface of GO, respectively. Pd-ZIF-8/rGO showed good catalytic activity in the Knoevenagel condensation-reduction tandem reaction of benzaldehyde and its substituted derivatives, which is due to the high catalytic activities of spatially separated Pd NPs and ZIF-8 active sites and the enriched reactants on the surface of Pd-ZIF-8/rGO due to the  $\pi$ - $\pi$  interaction between rGO and the reactants. The present approach provides a promising and universal strategy for the construction of hybrid catalysts based on MOFs, metal and GO materials for the tandem reaction.

### Acknowledgements

This work was financially supported by the National Natural Sciences Foundation of China (Nos.21776058 and 21236001), Natural Sciences Foundation of Hebei province (No.B2017202226 and E2015202306) and the Tianjin Municipal Natural Science Foundation (15JCYBJC21000) and Foundation of Education Bureau of Hebei Province (QN2016152). We thank to Prof. J. Zhao for helpful comments.

### References

- 1 A. Dhakshinamoorthy and H. Garcia, *Chem. Sus. Chem.*, 2014, **7**, 2392-2410.
- 2 D. Jagadeesan, *Appl. Catal. A Gen.*, 2016, **511**, 59-77.
- 3 I. B. Krylov and A. O. Terent'ev, *Russ. J. Org. Chem.*, 2015, **51**, 10-13.

- 4 Z. Zhang, J. Gao, J. J. Xia and G. W. Wang, *Org. Biomol. Chem.*, 2005, **3**, 1617-1619.
- 5 F. Tayyari, D. E. Wood and P. E. Fanwick, *Synthesis*, 2008, **2**, 0279-0285.
- 6 Y. Jia, Y. Fang, Y. Zhang, H. N. Miras and Y. F. Song, *Chem. Eur. J.*, 2015, **21**, 14862-14870.
- 7 S. Rana and S. B. Jonnalagadda, *Catal. Commun.*, 2017, **92**, 31-34.
- 8 G. B. Varadwaj, S. Rana and K. M. Parida, *Dalton Trans.*, 2013, **42**, 5122-5129.
- 9 L. Zhang, H. Wang, W. Z. Shen, Z. F. Qin, J. G. Wang and W. B. Fan, *J. Catal.*, 2016, **344**, 293-302.
- 10 H. F. Wang, C. Y. Wang, Y. F. Yang, M. Zhao and Y. J. Wang, *Catal. Sci. Technol.*, 2017, **7**, 405-417.
- 11 M. Opanasenko, A. Dhakshinamoorthy, M. Shamzhy, P. Nachtigall, M. Horáček, H. Garcia and J. Čejka, *Catal. Sci. Technol.*, 2013, **3**, 500-507.
- 12 R. Cortese and D. Duca, *Phys. Chem. Chem. Phys.*, 2011, **13**, 15995-16004.
- 13 D. K. Wang and Z. H. Li, *Catal. Sci. Technol.*, 2015, **5**, 1623-1628.
- 14 L. Y. Chen, B. H. Duan, Q. Luo, Z. Z. Gu, J. Liu and C. Y. Duan, *Catal. Sci. Technol.*, 2016, **6**, 1616-1620.
- 15 Y. R. Lee, M. S. Jang, H. Y. Cho, H. J. Kwon, S. Kim and W. S. Ahn, *Chem. Eng. J.*, 2015, **271**, 276-280.
- 16 U. P. N. Tran, K. K. A. Le and N. T. S. Phan, *ACS Catal.*, 2011, **1**, 120-127.
- 17 Y. Horiuchi, T. Toyao, M. Fujiwaki, S. Dohshi, T. H. Kim and M. Matsuoka, *RSC Adv.*, 2015, **5**, 24687-24690.
- 18 T. Zhang, X. F. Zhang, X. J. Yan, L. Y. Kong, G. C. Zhang, H. O. Liu, J. S. Qiu and K. L. Yeung, *Chem. Eng. J.*, 2013, **228**, 398-404.
- 19 F. Pang, M. Y. He and J. P. Ge, *Chem. Eur. J.*, 2015, **21**, 6879-6887.
- 20 C. Chizallet, S. Lazare, B.B. Delphine, F. Bonnier, V. Lecocq, E. Soyer, A. A. Quoineaud and N. Bats, *J. Am. Chem. Soc.*, 2010, **132**, 12365-12377.
- 21 Y. Zhao, M. M. Liu, B. B. Fan, Y. F. Chen, W. M. Lv, N. Y. Lu and R. F. Li, *Catal. Commun.*, 2014, **57**, 119-123.
- 22 X. Q. Jia, S. H. Wang and Y. Fan, *J. Catal.*, 2015, **327**, 54-57.
- 23 T. T. Dang, Y. Zhu, J. S. Y. Ngiam, S. C. Ghosh, A. Chen and A. M. Seayad, *ACS Catal.*, 2013, **3**, 1406-1410.
- 24 S. Rana, S. Maddila and S. B. Jonnalagadda, *Catal. Sci. Technol.*, 2015, **5**, 3235-3241.
- 25 S. Rana, S. Maddila, K. Yalagala and S. B. Jonnalagadda, *Appl. Catal. A Gen.*, 2015, **505**, 539-547.
- 26 S. Rana, S. Maddila, R. Pagadala and S. B. Jonnalagadda, *J. Porous Mat.*, 2015, **22**, 353-360.
- 27 M. Stürzel, F. Kempe, Y. Thomann, S. Mark, M. Enders and R. Mülhaupt, *Macromolecules*, 2012, **45**, 6878-6887.
- 28 G. Goncalves, P. A. A. P. Marques, C. M. Granadeiro, H. I. S. Nogueira, M. K. Singh and J. Grácio, *Chem. Mater.*, 2009, **21**, 4796-4802.
- 29 N. Morimoto, S.I. Yamamoto, Y. Takeuchi and Y. Nishina, *RSC Adv.*, 2013, **3**, 15608-15612.
- 30 S. I. Yamamoto, H. Kinoshita, H. Hashimoto and Y. Nishina, *Nanoscale*, 2014, **6**, 6501-6505.
- 31 R. Kumar, K. Jayaramulu, T. K. Maji and C. N. R. Rao, *Chem. Commun.*, 2013, **49**, 4947-4949.
- 32 Y. Zhou, L. Zhou, X. H. Zhang and Y. L. Chen, *Micropor. Mesopor. Mat.*, 2016, **225**, 488-493.
- 33 X. Huang, X. Qi, F. Boey and H. Zhang, *Chem. Soc. Rev.*, 2012, **41**, 666-686.
- 34 S. Bai and X. Shen, *RSC Adv.*, 2012, **2**, 64-98.
- 35 V. Georgakilas, M. Otyepka, A. B. Bourlinos, V. Chandra, N. Kim, K. C. Kemp, P. Hobza, R. Zboril and K. S. Kim, *Chem. Rev.*, 2012, **112**, 6156-6214.
- 36 J. H. Lee, J. Jaworski and J. H. Jung, *Nanoscale*, 2013, **5**, 8533-8540.
- 37 M. Wojtoniszak, X. C. Chen, R. J. Kalenczuk, A. Wajda, J. Lapczuk, M. Kurzewski, M. Drozdziak, P. K. Chu and E. B. Palen, *Colloid. surface. B.*, 2012, **89**, 79-85.
- 38 M. J. C. Ordoñez, K. J. Balkus, J. P. Ferraris and I. H. Musselman, *J. Membrane. Sci.*, 2010, **361**, 28-37.
- 39 J. F. Yao, R. Z. Chen, K. Wang and H. T. Wang, *Micropor. Mesopor. Mat.*, 2013, **165**, 200-204.
- 40 S. Luanwuthi, A. Krittayavathananon, P. Srimuk and M. Sawangphruk, *RSC Adv.*, 2015, **5**, 46617-46623.
- 41 Y. Hu, H. Kazemian, S. Rohani, Y. Huang and Y. Song, *Chem. Commun.*, 2011, **47**, 12694-12696.

- 42 Z. J. Fan, P. Song, F. Wei, W. Kai, J. Yan, T. Wei, L. J. Zhi, J. Feng, Y. M. Ren, L. P. Song and F. Wei, *ACS Nano.*, 2011, **5**, 191-198.
- 43 H. J. Shin, K. K. Kim, A. Benayad, S. M. Yoon, H. K. Park, I. S. Jung, M. H. Jin, H. K. Jeong, J. M. Kim, J. Y. Choi and Y. H. Lee, *Adv. Funct. Mater.*, 2009, **19**, 1987-1992.
- 44 S. Moussa, A. R. Siamaki, B. F. Gupton and M. S. El-Shall, *ACS Catal.*, 2012, **2**, 145-154.
- 45 Y. Matsuo, T. Miyabe, T. Fukutsuka and Y. Sugie, *Carbon*, 2007, **45** 1005-1012.
- 46 K. S. Park, Z. Ni, A. P. Cote, J. Y. Choi, R. Huang, F. J. Uribe-Romo, H. K. Chae, M. O'Keeffe and O. M. Yaghi, *P. Natl. Acad. Sci. USA*, 2006, **103**, 10186-10191.
- 47 Z. J. Bian, S. P. Zhang, X. M. Zhu, Y. K. Li, H. L. Liu and J. Hu, *RSC Adv.*, 2015, **5**, 31502-31505.
- 48 D. Y. Cai and M. Song, *J. Mater. Chem.*, 2007, **17**, 3678-3680.
- 49 S. R. Venna, J. B. Jasinski and M. A. Carreon, *J. Am. Chem. Soc.* 2010, **132**, 18030-18033.
- 50 J. Wang, Y. M. Wang, Y. T. Zhang, A. A. Uliana, Z. Y. Zhu, J. D. Liu and B. V. D. Bruggen, *ACS Appl. Mater. Inter.*, 2016, **38**, 25508-25519.
- 51 H. Zhou, J. Zhang, J. Zhang, X. F. Yan, X. P. Shen and A. H. Yuan, *Int. J. Hydrogen Ener.*, 2015, **40**, 12275-12285.
- 52 S. S. Ding, Q. Yan, H. Jiang, Z. X. Zhong, R. Z. Chen and W. H. Xing, *Chem. Eng. J.*, 2016, **296**, 146-153.
- 53 C. Petit and T. J. Bandosz, *Adv. Funct. Mater.*, 2011, **21**, 2108-2117.
- 54 T. Wu, X. R. Wang, H. X. Qiu, J. P. Gao, W. Wang and Y. Liu, *J. Mater. Chem.*, 2012, **22**, 4772-4779.
- 55 M. Sawangphruk, P. Srimuk, P. Chiochan, T. Sangsri and P. Siwayaprahm, *Carbon*, 2012, **50**, 5156-5161.
- 56 J. Xu, S. He, H. L. Zhang, J. C. Huang, H. X. Lin, X. X. Wang and J. L. Long, *J. Mater. Chem. A*, 2015, **3**, 24261-24271.
- 57 C. Zhang, L. L. Ren, X. Y. Wang and T. X. Liu, *J. Phys. Chem. C*, 2010, **114**, 11435-11440.
- 58 M. Jahan, Z. L. Liu and K. P. Loh, *Adv. Funct. Mater.*, 2013, **23**, 5363-5372.
- 59 B. L. Chen, Y. Q. Zhu and Y. D. Xia, *RSC Adv.*, 2015, **5**, 30464-30471.
- 60 C. H. Kuo, Y. Tang, L. Y. Chou, B. T. Sneed, C. N. Brodsky, Z. Zhao and C. K. Tsung, *J. Am. Chem. Soc.*, 2012, **134**, 14345-14348.
- 61 Y. W. Liu, M. X. Guan, L. Feng, S. L. Deng, J. F. Bao, S. Y. Xie, Z. Chen, R. B. Huang and L. S. Zheng, *Nanotechnology*, 2013, **24**, 025604-025613.
- 62 S. Some, Y. Kim, E. Hwang, H. Yoo and H. Lee, *Chem. Commun.*, 2012, **48**, 7732-7734.
- 63 Z. M. Wang, C. L. Xu, G. Q. Gao and X. Li, *RSC Adv.*, 2014, **4**, 13644-13651.
- 64 X. Yan, Q. Q. Li and L. S. Li, *J. Am. Chem. Soc.*, 2012, **134**, 16095-16098.
- 65 V. G. Deshman, S. L. Owen, R. Y. Abrokwhah and D. Kuila, *J. Mol. Catal., A-Chem.* 2015, **408**, 202-213.
- 66 W. J. Shen, M. Okumura, Y. Matsumura and M. Haruta, *Appl. Catal. A-Gen.*, 2001, **213**, 225-232.
- 67 Z. Gao, M. Dong, G. Z. Wang, P. Sheng, Z. W. Wu, H. M. Yang, B. Zhang, G. F. Wang, J. G. Wang and Y. Qin, *Angew. Chem. Int. Ed.*, 2015, **54**, 9006-9010.
- 68 F. M. Zhang, Y. Jin, Y. H. Fu, Y. J. Zhong, W. D. Zhu, A. A. Ibrahim and M. S. El-Shall, *J. Mater. Chem. A*, 2015, **3**, 7008-17015.
- 69 Y. F. Yang, F. W. Wang, Q. H. Yang, Y. L. Hu, H. Yan, Y. Z. Chen, H. R. Liu, G. Q. Zhang, J. L. Lu, H. H. Jiang and H. X. Xu, *ACS Appl. Mater. Interfaces* 2014, **6**, 18163-18171.
- 70 N. R. Wilson, Z. Liu, P. A. Pandey, K. Suenaga, R. Beanland, J. P. Rourke, R. J. Young, S. J. York, J. Sloan, I. A. Kinloch and L. Gong, *ACS Nano.*, 2009, **3**, 2547-2556.
- 71 Y. C. Pan, Y. Y. Liu, G. F. Zeng, L. Zhao and Z. P. Lai, *Chem. Commun.*, 2011, **47**, 2071-2073.
- 72 G. Lu, S. Z. Li, Z. Guo, O. K. Farha, B. G. Hauser, X. Y. Qi, Y. Wang, X. Wang, S. Y. Han, X. G. Liu, J. S. D. Chene, H. Zhang, Q. C. Zhang, X. D. Chen, J. Ma, S. C. J. Loo, W. D. Wei, Y. H. Yang, J. T. Hupp and F. W. Huo, *Nat. Chem.*, 2012, **4**, 310-316.
- 73 F. M. Zhang, S. Zheng, Q. Xiao, Y. J. Zhong, W. D. Zhu, A. Lin, and M. S. El-Shall, *Green Chem.*, 2016, **18**, 2900-2908.
- 74 M. B. Ansari, H. L. Jin, M. N. Parvin and S. E. Park, *Catal. Today*, 2012, **185**, 211-216.
- 75 L. Xu, C. G. Li, K. Zhang and Wu, *ACS Catal.*, 2014, **4**, 2959-2968.

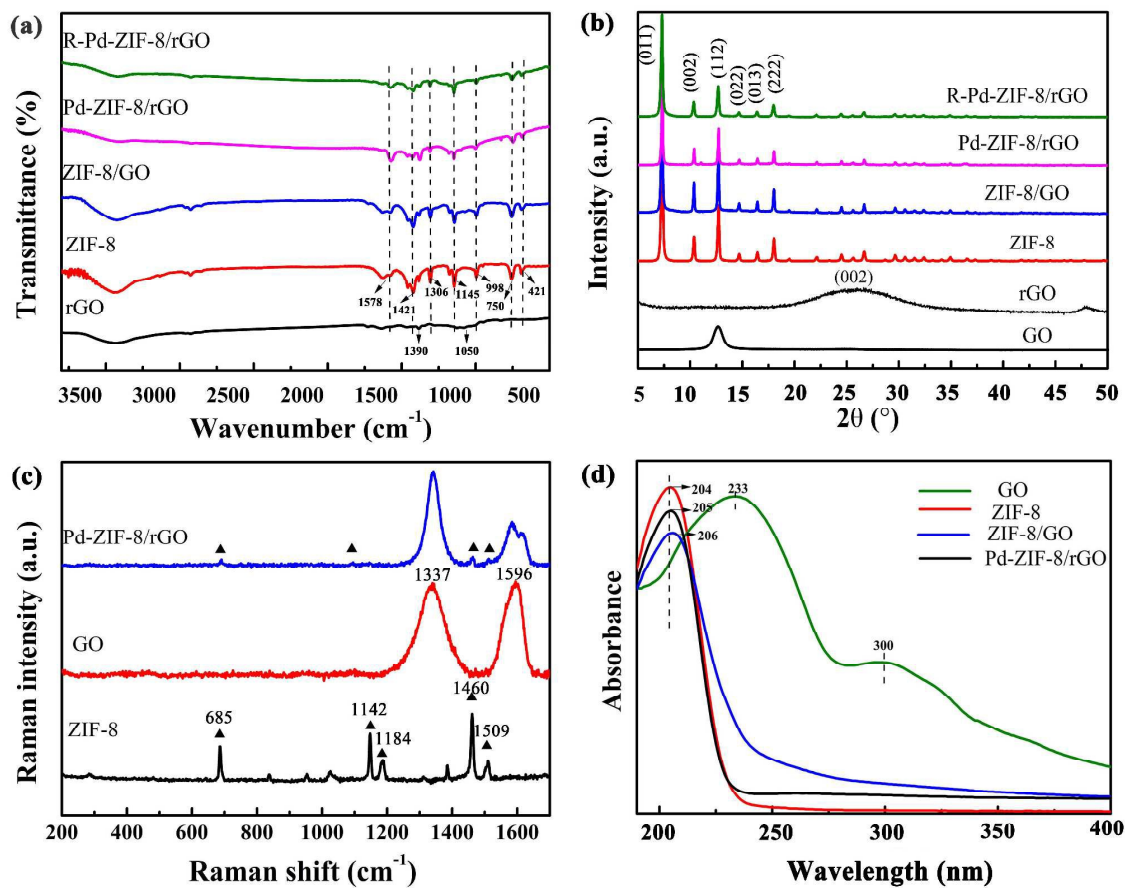


**Fig. 1.** FTIR spectra of rGO, ZIF-8, ZIF-8/GO, Pd-ZIF-8/rGO and R-Pd-ZIF-8/rGO (a), XRD patterns of GO, rGO, ZIF-8, ZIF-8/GO, Pd-ZIF-8/rGO and R-Pd-ZIF-8/rGO (b), Raman spectra of GO, ZIF-8 and Pd-ZIF-8/rGO (c) and UV-Vis spectra of GO, ZIF-8, ZIF-8/GO and Pd-ZIF-8/rGO (d).

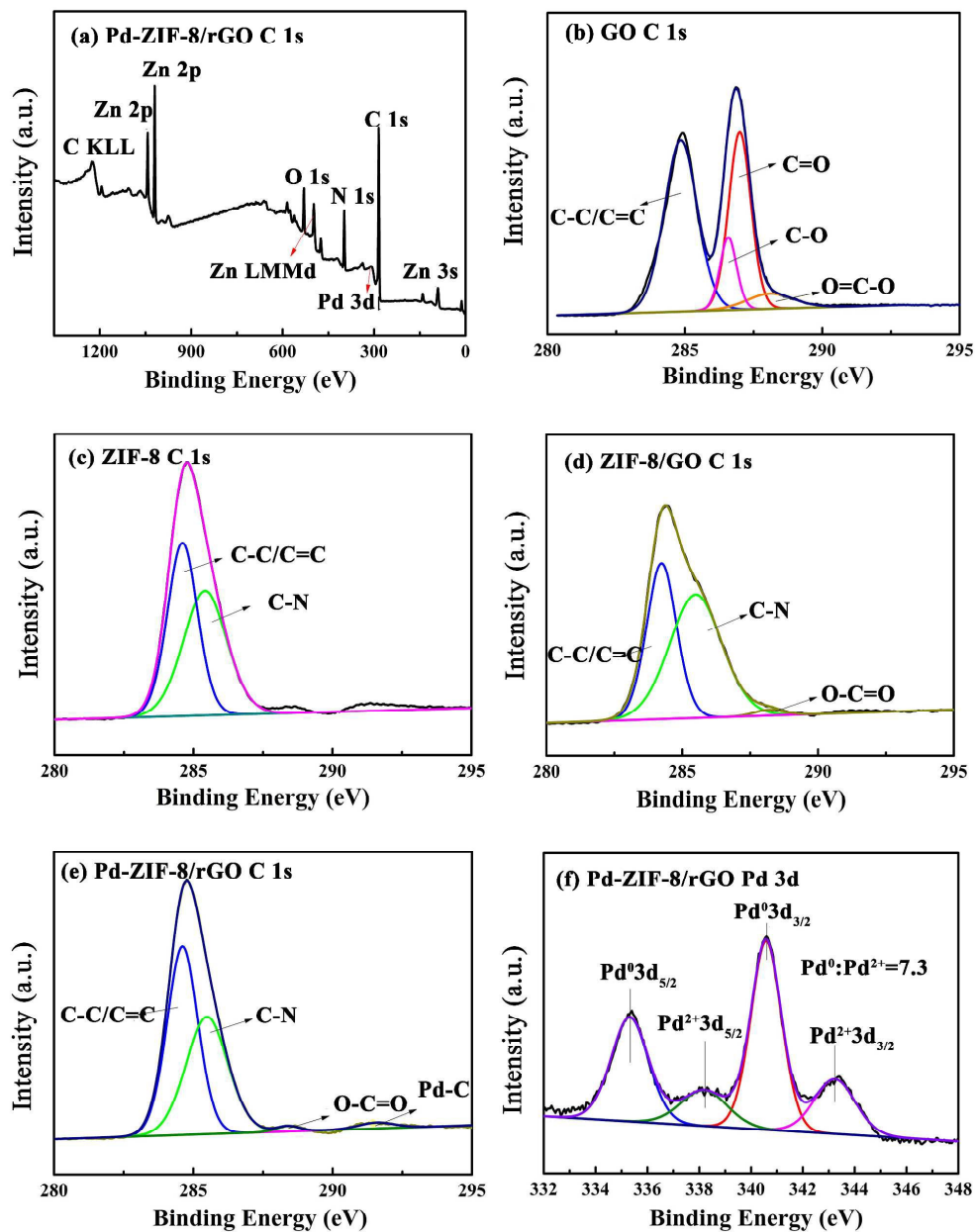


Fig. 2. XPS wide scan spectra of Pd-ZIF-8/rGO (a) and C 1s XPS spectra of GO (b), ZIF-8 (c), ZIF-8/GO (d), Pd-ZIF-8/rGO (e) and Pd 3d XPS spectra of Pd-ZIF-8/rGO (f).

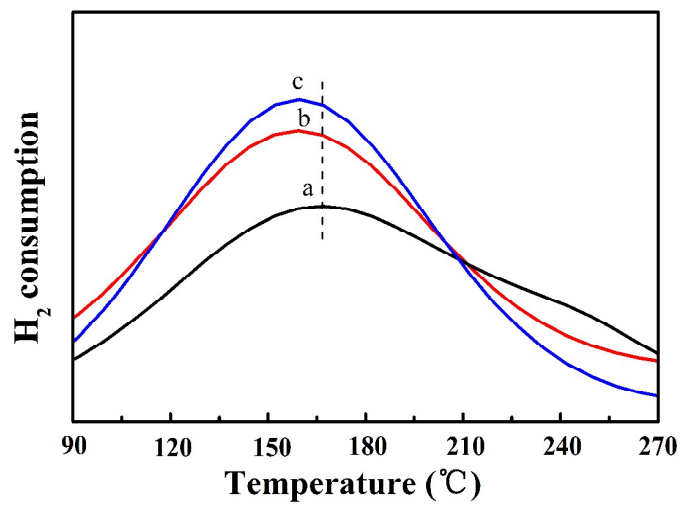


Fig. 3. H<sub>2</sub>-TPR profiles of Pd/ZIF-8 (a), Pd/(ZIF-8+rGO) (b) and Pd-ZIF-8/rGO (c).

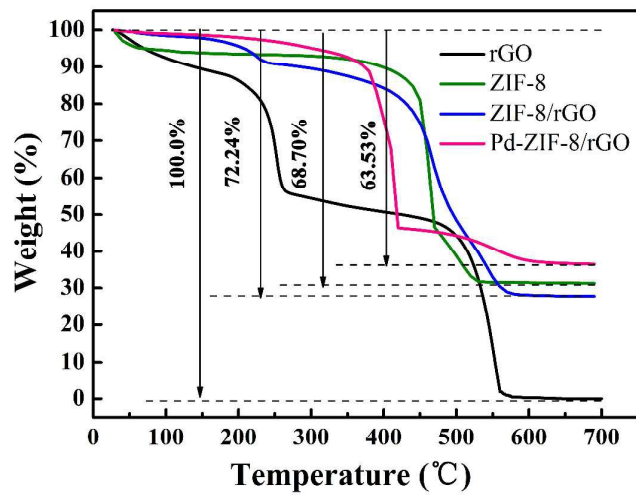
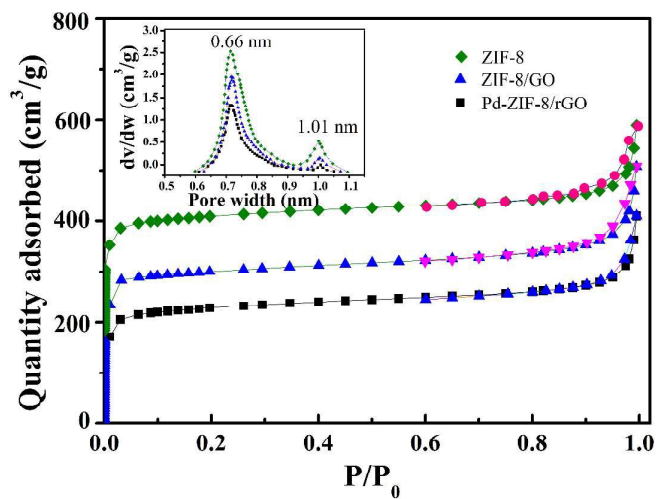
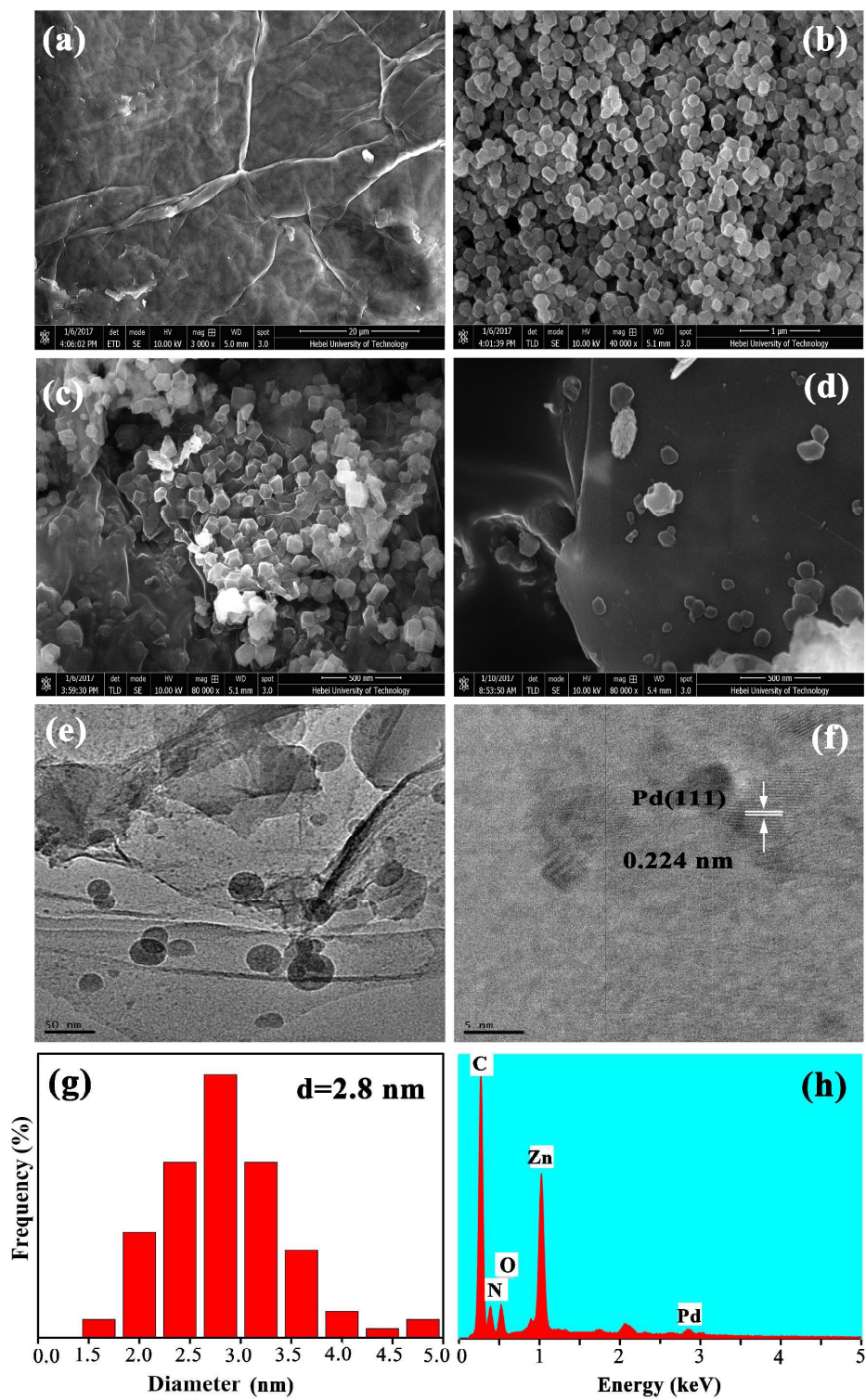


Fig. 4. The TGA curves of rGO, ZIF-8, ZIF-8/rGO and Pd-ZIF-8/rGO.



**Fig. 5.** N<sub>2</sub> adsorption-desorption isotherms of ZIF-8, ZIF-8/GO and Pd-ZIF-8/rGO and the corresponding pore-size distributions calculated by the Horvath-Kawazoe method (inset).



**Fig. 6.** SEM images of GO (a), ZIF-8 (b), ZIF-8/GO (c) and Pd-ZIF-8/rGO (d), TEM images of Pd-ZIF-8/rGO (e, f), the size distribution plot of Pd NPs (g) and EDS image of Pd-ZIF-8/rGO (h)

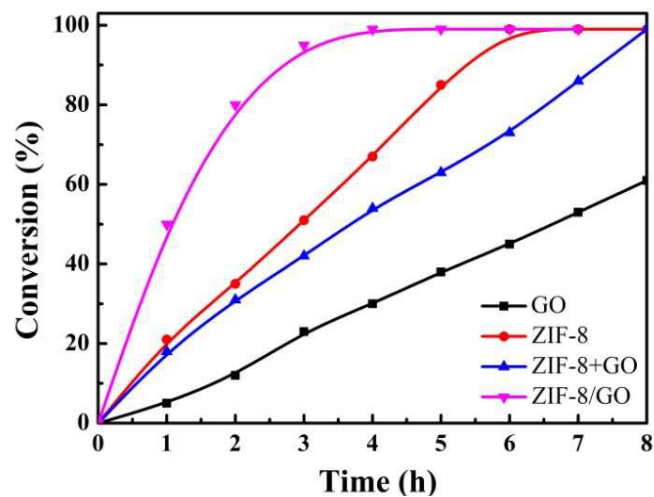


**Fig. 7.** Knoevenagel condensation of benzaldehyde with malononitrile over different catalysts. Reaction conditions:  $A_1$  (1.9 mmol), toluene (5.0 mL), malononitrile (3.8 mmol), 25 °C, 8.0 h. catalyst: GO 10 mg, ZIF-8 30 mg, physical mixture of ZIF-8 30 mg and GO 10.0 mg and ZIF-8/GO (the weight percentage of ZIF-8 is 75.0%) 40.0 mg.

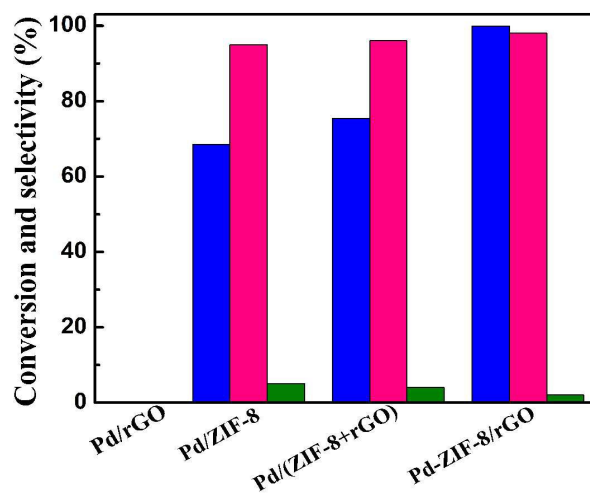


**Fig. 8.** The tandem reaction of Knoevenagel-reduction, conversion of A<sub>1</sub> (blue), selectivity to C<sub>1</sub> (pink) and selectivity to B<sub>1</sub> (green). Reaction conditions: A<sub>1</sub> (1.9 mmol), toluene (5 mL), malononitrile (3.8 mmol), catalyst: Pd/rGO 10 mg, Pd/ZIF-8 30 mg, Pd/(ZIF-8+rGO) 40 mg and Pd-ZIF-8/rGO 40 mg. Condensation was carried out at 60 °C for 4.0 h; reduction was carried out at atmospheric pressure with H<sub>2</sub> and at 60 °C for 12.0 h.

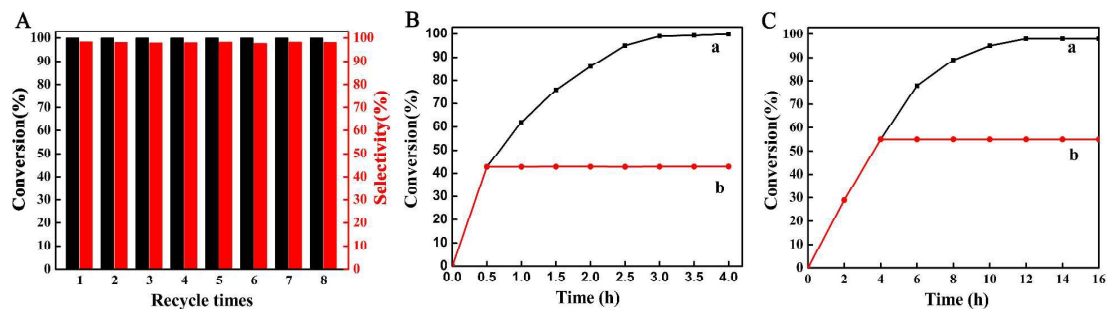


**Fig. 9.** (A) Recyclability test of the Pd-ZIF-8/rGO catalyst; (B) Hot filtration experiments for Knoevenagel condensation reaction: (a) with the presence of Pd-ZIF-8/rGO; (b) Pd-ZIF-8/rGO was hot filtrated at 0.5 h; (C) Hot filtration experiments for reduction reaction: (a) with the presence of Pd-ZIF-8/rGO; (b) Pd-ZIF-8/rGO was hot filtrated at 5.0 h.

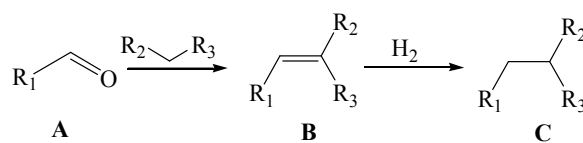
**Table 1.** Textural parameters of ZIF-8, ZIF-8/GO and Pd-ZIF-8/rGO

Sample	BET Surface Area (m <sup>2</sup> /g)	Langmuir Surface Area	External Surface Area	Micropore Volume (cm <sup>3</sup> /g)	Pore Width
ZIF-8	1417	1876	146	0.58	0.66
ZIF-8/GO	757	1001	135	0.31	0.66
Pd-ZIF-8/rGO	578	766	130	0.28	0.66

**Table 2.** CO characteristics of Pd/ZIF-8, Pd/(ZIF-8+rGO) and Pd-ZIF-8/rGO

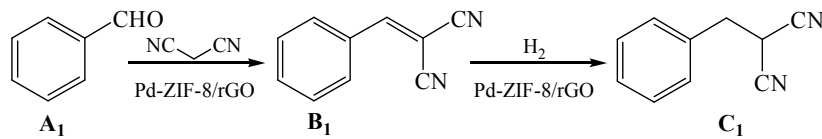
Catalyst	Pd loading (wt.%) <sup>a</sup>	Pd dispersion (%) <sup>b</sup>	Particle size (nm) <sup>b</sup>	CO adsorption (μmol/g)
Pd/ZIF-8	11.9	7.68	12.9	85.9
Pd/(ZIF-8+rGO)	13.2	11.2	9.81	138.9
Pd-ZIF-8/rGO	12.5	31.0	3.20	364.2

<sup>a</sup> Determined by ICP.<sup>b</sup> Calculated according to CO uptake.

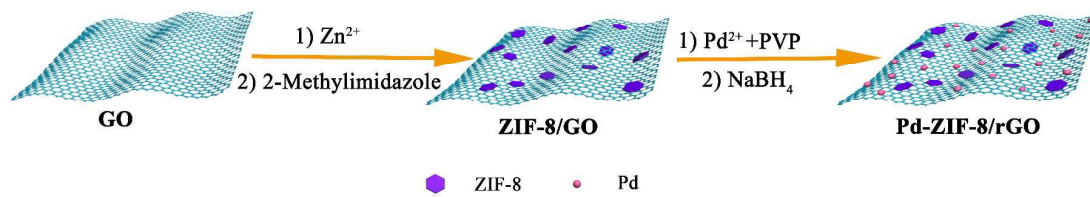
**Table 3.** Knoevenagel condensation-reduction tandem reactions with different substrates over Pd-ZIF-8/rGO

Entry	A	R <sub>2</sub>	R <sub>3</sub>	Time (h)	Conversion A (%)	Selectivity (%)	
						C	B
1		CN	CN	4+12	99.9	98.3	1.7
2		CN	CN	5+12	99.9	96.7	3.3
3		CN	CN	5+12	99.9	92.5	7.5
4		CN	CN	5+12	99.9	93.2	6.8
5		CN	CN	3+12	99.9	91.2	8.8
6		CN	CN	3+12	99.9	92.8	7.2
7		CN	COOEt	6+12	87.6	92.3	7.7
8		COOEt	COOEt	6+12	78.5	88.6	11.4

Reaction conditions: A (1.9 mmol), toluene (5 mL), 60 °C, active methylene compound (3.8 mmol), Pd-ZIF-8/rGO 150 mg.



**Scheme 1.** One-pot tandem Knoevenagel condensation-reduction reaction over Pd-ZIF-8/rGO.



**Scheme 2.** Illustration of the preparation of Pd-ZIF-8/rGO catalyst.

## Table of contents entry

A novel bifunctional catalyst for Knoevenagel condensation-reduction tandem reaction was prepared by immobilizing ZIF-8 and Pd on GO, respectively.

